In-plane and out-of-plane compressive properties of regular and graded cellular cores of sandwich panels fabricated by additive manufacturing

Bernardo Coelho, Etienne Copin, Augusto Moita Deus, Maria Fatima Vaz

▶ **To cite this version:**

Bernardo Coelho, Etienne Copin, Augusto Moita Deus, Maria Fatima Vaz. In-plane and out-of-plane compressive properties of regular and graded cellular cores of sandwich panels fabricated by additive manufacturing. Proceedings of the Institution of Mechanical Engineers, Part L: Journal of Materials: Design and Applications, 2025, 239 (1), pp.165-179. ⟨10.1177/14644207241255632⟩. ⟨hal-04584760⟩

HAL Id: hal-04584760

https://imt-mines-albi.hal.science/hal-04584760v1

Submitted on 4 Jun 2024

HAL is a multi-disciplinary open access archive for the deposit and dissemination of scientific research documents, whether they are published or not. The documents may come from teaching and research institutions in France or abroad, or from public or private research centers.

L'archive ouverte pluridisciplinaire **HAL**, est destinée au dépôt et à la diffusion de documents scientifiques de niveau recherche, publiés ou non, émanant des établissements d'enseignement et de recherche français ou étrangers, des laboratoires publics ou privés.

HAL Authorization

In-plane and out-of-plane compressive properties of regular and graded cellular cores of sandwich panels fabricated by additive manufacturing

Bernardo Coelho[1], Etienne Copin[2], Augusto Moita Deus[3,4] and Maria Fatima Vaz[1,3]

Abstract

Cellular materials with a gradient of properties become appealing as cores of the sandwich panels due to the possibility of improving strength and absorbed energy in lightweight components. 2D cellular structures designated by honeycombs have an anisotropic behaviour when loaded under in- and out-plane. Thus, when proposing new designs, it is essential to analyse how the in-plane arrangement with a gradient in cell wall thickness affects in-plane and out-of-plane mechanical properties. This work aims to study graded cellular structures in comparison with regular hexagonal honeycombs. Structures were manufactured by laser powder bed fusion using an aluminium alloy. Regular arrangements were formed with cells with the same thickness, while graded structures possessed a radial gradient of cell thickness. Three types of innovative gradients, where cell length varies radially along concentric layers, were analysed. The compressive properties of regular and graded structures were evaluated when loaded both under in-plane and out-of-plane conditions. Compression behaviour was assessed, both experimentally and by numerical modelling. Even though there is a mismatch between numerical and experimental results, they exhibit the same trends. All graded samples showed an increased mechanical performance when loaded under out-of-plane conditions in comparison with the results from tests under in-plane loading with values, for example, of stiffness four hundred times larger, absorbed energy around thirty times higher and with yield stress four times larger. The results showed that the graded samples attain higher values of strength, stiffness and absorbed energy in comparison with regular hexagonal honeycombs, for the same relative density.

Highlights

- Cellular structures with radial cell length gradients were designed and fabricated by L-PBF.
- Regular and graded samples were compressed under in-plane and out-of-plane loadings
- Numerical simulations carried out with a finite element model were compared with the experimental results.
- The mechanical response of the graded samples, namely the strength and absorbed energy, was enhanced in comparison with the regular ones.

Introduction

Sandwich panels comprising honeycomb cores have been widely used in engineering application fields such as aerospace, automotive, transportation, civil construction and sporting equipment.[1] Two thin sheets and a thicker cellular core compose a sandwich panel. The role of the core is to increase the stiffness and to reduce the stresses in the panel.[2]

[1]IDMEC, Instituto Superior Técnico, Universidade de Lisboa, Lisboa, Portugal

[2]Institut Clément Ader (ICA), Université de Toulouse, CNRS, IMT Mines Albi, INSA, ISAE-SUPAERO, UPS, Albi, France

[3]Departamento de Engenharia Mecânica, Instituto Superior Técnico, Universidade de Lisboa, Lisboa, Portugal

[4]CEFEMA, Instituto Superior Técnico, Universidade de Lisboa, Lisboa, Portugal

The most common cell topology of the core is regular hexagonal honeycomb, which is a two-dimensional cellular structure that possesses high specific stiffness, specific strength, and specific absorbed energy, in comparison to the same solid material with the same mass.[2] Several studies involving different loading conditions were have been conducted to analyse both in-plane and out-of-plane properties of the honeycomb structures.[2–8] Under compression, regular hexagonal honeycombs exhibit high stiffness and strength when loaded in the out-of-plane direction, because the deformation occurs through the compression of the cell walls.[2] In contrast, the in-plane stiffness and strength of regular honeycomb structures are much lower due to the bending of the cell walls.[2]

Recently, new design approaches have been proposed due to the growing demands of higher absorbed energy, thus more complex cell shapes have been studied, resulting in modified honeycombs.[9–12] By exploring new cell designs, researchers also try to improve the in-plane properties of the honeycombs, which exhibit lower values than the ones obtained under out-of-plane testing. Different cells topologies have been developed based on truss lattices, with atomic-based arrays, or based on Kelvin, rhombicuboctahedron, pyramidal, diamond cubic and octahedral unit cells, or triply periodic minimal surfaces, among others.[13–20]

The concept of gradient was introduced aiming to increase the performance of the honeycombs.[21,22] Gradients may be defined by changing the material properties,[23] or cell size[24] or cell wall thickness.[21,25–30] Graded design affects the deformation of the honeycombs, being localized at the moving block, while the deformation pattern of the regular hexagonal honeycombs, occurs inside the sample.[30] In addition, honeycombs with a graded in-plane arrangement were found to have enhanced crushing strength and energy absorption in the out-of-plane directions, in comparison with the properties of regular honeycombs.[22]

The growing interest in additive manufacturing (AM) over the last decade mainly lies in the freedom of design and the gain in time between the design and the production of parts, as it allows to make objects from a 3D model data, layer by layer and without the need of molds.[31] In this perspective, metallic additive manufacturing technologies enable the rapid experimental investigation of the mechanical behaviour of various advanced honeycomb structures with complex shape, such as graded cellular structures. Among metal AM technologies, laser powder bed fusion (L-PBF) is one of the most commonly used for metals[6,32] especially to print parts made of aluminum alloys. Although, the most used core material is aluminium, natural base materials such as vinylester matrix reinforced with jute fabric, or polypropylene with sisal fibres are becoming common.[1,6,33] As AM technologies deposits material directionally, the result is a part that has an anisotropic behaviour.[34–36] However, it is common to assume that the material properties are isotropic.

The aim of this research was to investigate the mechanical performance of new aluminum in-plane graded honeycomb structures fabricated by additive manufacturing method, namely L-PBF. The purpose is to increase the efficiency of sandwich panel cores regarding strength-to-weight ratio, with new radial in-plane gradients that help to improve both the in- and out-of-plane properties of the structures. Samples were designed with a radial gradient, meaning that the cell length varies radially, along concentric layers. Experimental compression tests and numerical simulations by the finite element analysis method were carried out, both under in-plane and out-of-plane directions to assess the influence of the in-plane gradient, and to compare with regular structures. The mechanical responses including strength, stiffness, absorbed energy and failure modes were analysed.

Materials and methods

Materials

Due to the complex geometry of the honeycomb structures, an additive process was selected to produce the aluminum samples, namely laser powder bed fusion, as it was not possible to fabricate the specimens with a more conventional procedure. L-PBF is one of the most common manufacturing methods for this type of samples with small size and complex geometry. The material used was an aluminum cast alloy, AlSi7Mg0.6, described as EN AC-42200 (DIN EN 1706), acquired from SLM Solutions GMBH, Lübeck, Germany. The particle size of the metallic powders was comprised between 20 and 63 μm. The physical and mechanical properties, such as, density ρ, Young's modulus E, Poisson's ratio ν, yield strength σ_Y, ultimate strength σ_U, and ultimate strain ϵ_U were taken, respectively as, $\rho = 2.68\,g/cm^3$, $E = 59$ GPa, $\nu = 0.33$, $\sigma_Y = 212$ MPa, $\sigma_U = 405$ MPa, $\epsilon_U = 0.07$.[37,38]

Honeycomb structures

The honeycomb structures were drawn using the 3D CAD program SolidWorks (SolidWorks 2018). Two sets of honeycomb structures were studied, in particular, regular and graded. For regular honeycombs all cells have the same thickness, while on graded honeycombs there are differences in the cell thickness.

Regular honeycombs were drawn with the geometrical parameters defined, for each unit cell, of Figure 1(a), namely the cell length l, the wall thickness t and the cell height h. Figure 1(b) exemplifies a regular honeycomb sample, with the dimensions s_1 and s_2. All regular structures were designed keeping the thickness fixed as $t = 2.31$ mm, as in a previous work,[6] while the parameters l and h were varied. The cell wall length took the values of 6, 8, and 10 mm. For each structure with a set value of cell wall length, the cell height was varied between 6, 10 and 12 mm, resulting in nine different structures (Table 1). The designation of the samples includes the cell length and the cell height, for which, for example, L6H6 stands for $l = 6$ mm and $h = 6$ mm. Examples of regular honeycombs specimens L6H10, L8H10 and L10H10 are given in Figure 2.

One of the most important properties of the cellular materials is the relative density, $\bar{\rho}$ which is defined as

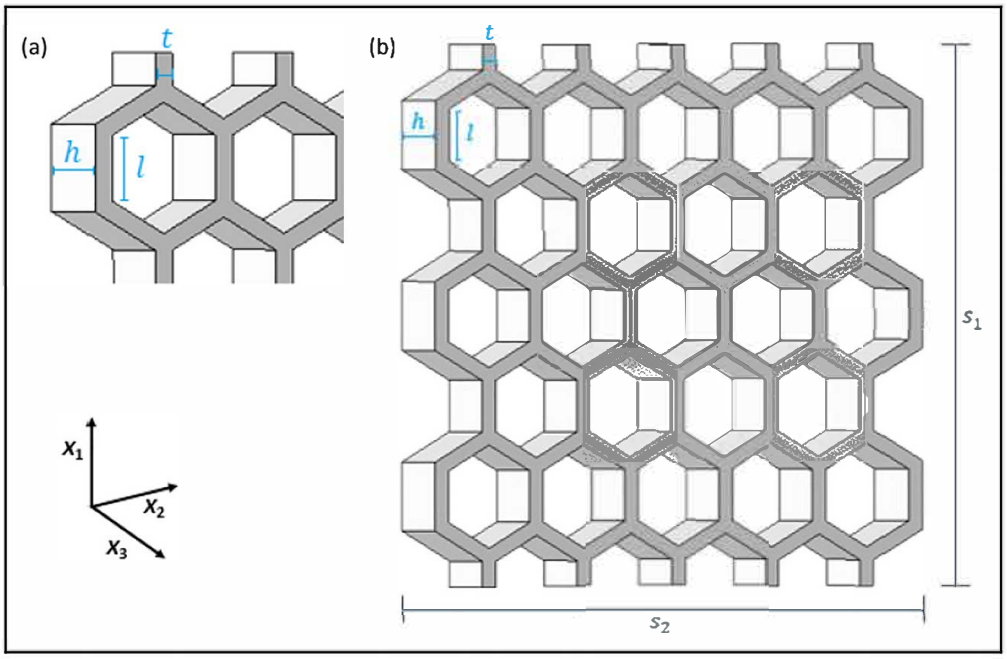

Figure 1. (a) Parameters of cell; (b) dimensions of the sample.

Table 1. Designation, geometrical parameters and relative density $\bar{\rho}$ for the regular structures with a constant thickness $t = 2.31$ mm.

Designation	l (mm)	h (mm)	s_1 (mm)	s_2 (mm)	$\bar{\rho}$
L6H6	6	6	66	66	0.338
L6H10	6	10	66	66	
L6H12	6	12	66	66	
L8H6	8	6	83	84	0.269
L8H10	8	10	83	84	
L8H12	8	12	83	84	
L10H6	10	6	61	68	0.228
L10H10	10	10	61	68	
L10H12	10	12	61	68	

the ratio between the density of cellular material and the density of the compact material that forms the cell walls or struts.[2] The relative density for all regular samples is presented in Table 1.

Graded samples were drawn with three different gradient types, keeping the cell height $h = 12$ mm. The designation for each graded structure depends on its gradient group, being samples with gradient 1, assigned with the designations 1A and 1B, respectively. The same applies to the remaining gradient types.

A radial gradient was constructed meaning that equal cell thickness was found in equally distanced concentric layers centred in the central cell. The thickness changes discretely from layer to layer. For example, graded sample 1A has an increasing cell length, meaning that the central cell has $l = 6$ mm, while the layer that surrounds it has $l = 8$ mm. A third layer is designed with $l = 10$ mm. Finally, as the purpose is to have a square sample, the specimen is filled with cells with $l = 8$ mm. While graded sample 1A was built with increasing cell length (l:6→8→10) from the centre and consequent decreasing cell wall thickness, sample 1B was designed with decreasing cell length (l:10→8→6) and consequent increasing cell wall thickness (Figure 3). The designation, the geometrical parameters, and the relative density of graded samples 1A and 1B are presented in Table 2.

The construction of graded type 2 samples was based on increments of the cell length. For graded samples 2A and 2B, the central cell was designed with $l = 7$ mm, while the cell length progressively increases by an increment of 0.5 mm for each concentric layer. Two different structures were developed differing solely on the cell wall length of the four cells in the corners, being of 8.5 and of 7 mm in samples 2A and 2B, respectively. Samples 2C and 2D have central cell wall lengths of 9 mm, progressively decreasing by an increment of 0.5 mm with each concentric layer. Samples 2C and 2D differ only in the cell wall length of the four cells in the corners, having the values of 7.5 and of 8.5 mm in samples 2C and 2D, respectively. The characteristics of graded type 2 structures are presented in Table 3, while Figure 4 exhibits their schematic representations.

Graded type 3 samples were designed considering the gradient of cell thickness parameter, G, defined in a previous work.[21] This parameter is calculated from the initial and final values chosen for cell wall thickness and cell length, with the density gradient emerging from the slope of the size function. Positive G parameters indicate that the thickness of the cells increases towards the central cell, while negative G indicates the opposite. Graded type 3 samples are exhibited in Figure 5, while their geometrical parameters are given in Table 4. Samples have a different notation from the previous ones, where n and p stand, respectively, for negative and positive values of the G parameter. Three values of G were investigated, corresponding to the 3A, 3B and 3C samples, with their positive/negative variants.

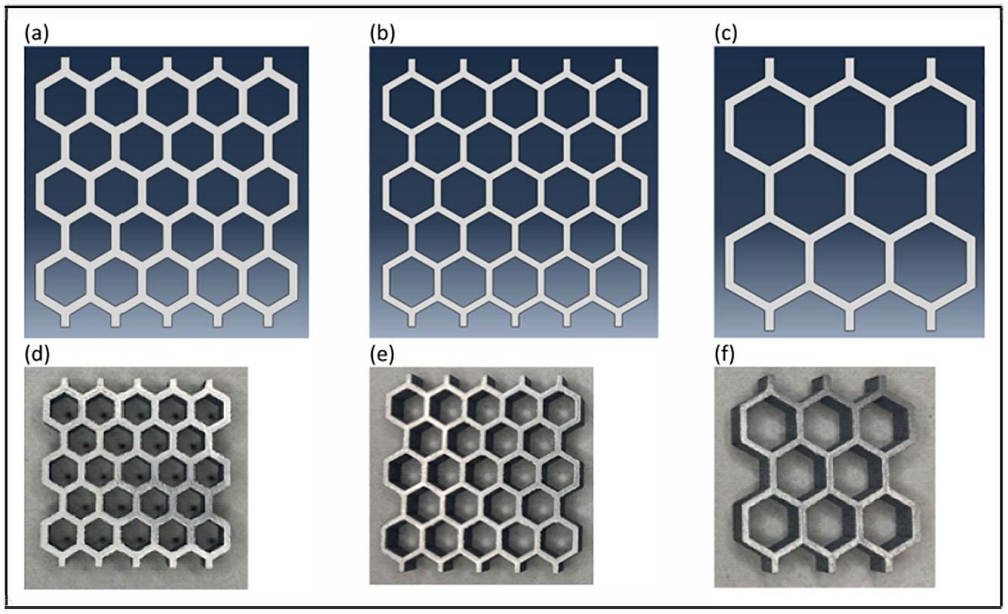

Figure 2. Regular hexagonal honeycomb samples with a constant thickness $t = 2.31$ mm. Schematic representation and printed aluminium samples (a)(d) L6H10, (b)(e) L8H10, (c)(f)L10H10.

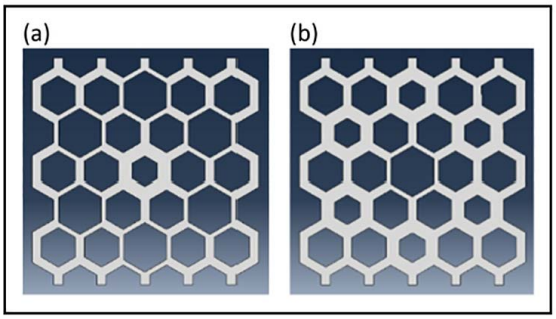

Figure 3. Schematic representation of graded type 1 samples with a constant height of $h = 12$ mm. The cell length varies radially among concentric layers. (a) sample 1A and (b) sample 1B.

Table 2. Designation, geometrical parameters and relative density $\bar{\rho}$ for the graded type 1 structures with a constant height $h = 12$ mm. The cell length l varies radially along concentric layers.

Designation	*l variation* (mm)	s_1 (mm)	s_2 (mm)	$\bar{\rho}$
1A	6→8→10	92	91	0.322
1B	10→8→6	92	91	0.421

Manufacturing

The aluminum samples were produced by the L-PBF process, on a SLM Solutions 125HL machine (SLM Solutions GMBH, Lübeck, Germany) available at the Institut Clément Ader (ICA), IMT Mines Albi, France. It is equipped with a 400-W Yb laser (1075 µm) with a Gaussian-beam-focus diameter of 70–100 µm. The process took place in a chamber filled with argon (partial pressure of oxygen kept below 0.1 at.%), to limit material oxidation. Furthermore, a constant flow of argon was maintained over the powder bed during the fabrication to further protect the parts from oxidation and blow away the spatters. The building platform was held at a temperature of 150°C throughout the whole process to reduce thermal stresses. The scanning strategy included contours and used a stripe fill pattern, including a strip length of 10 mm and a rotation angle of 67° between consecutive layers.[39] A hatch spacing of 170 µm and a layer thickness of 50 µm were selected for all the L-PBF processed materials.[39] Volume process parameters used a laser power of 350 W and a scanning speed of 1150 mm/s. Contouring parameters used a laser power of 300 and 250 W, with a scan speed of 600 and 555 mm/s for the outer contour and the inner contour, respectively. For the latter, the laser focus was set at −4 mm. These parameters correspond to standard parameters recommended by SLM Solutions.[39] For each fabrication, 3 to 6 identical samples were made on top of each other to make use of the building volume of the machine. After the fabrication, the samples were separated from the building plate. Vertical surfaces were left in the as-built state, while the bottom and top horizontal surfaces were grinded with SiC paper to remove the remaining traces of supports.

Table 3. Designation, geometrical parameters and relative density $\bar{\rho}$ for the graded type 2 structures with a constant height $h = 12$ mm.

Designation	*l variation* (mm)	Corner dimension (mm)	s_1 (mm)	s_2 (mm)	$\bar{\rho}$
2A	7 + 0.5	8.5	100	102	0.443
2B	7 + 0.5	7	100	102	0.466
2C	9–0.5	7.5	100	102	0.426
2D	9–0.5	8.5	100	102	0.410

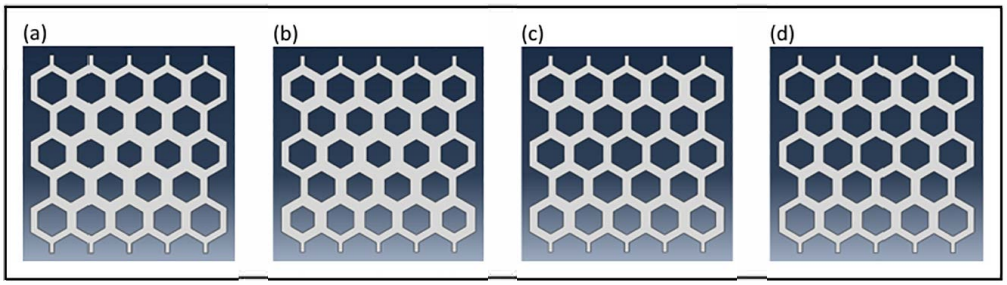

Figure 4. Graded type 2 samples with a constant height of $h = 12$ mm. The cell length varies radially among concentric layers. (a) 2A; (b) 2B; (c) 2C; (d) 2D.

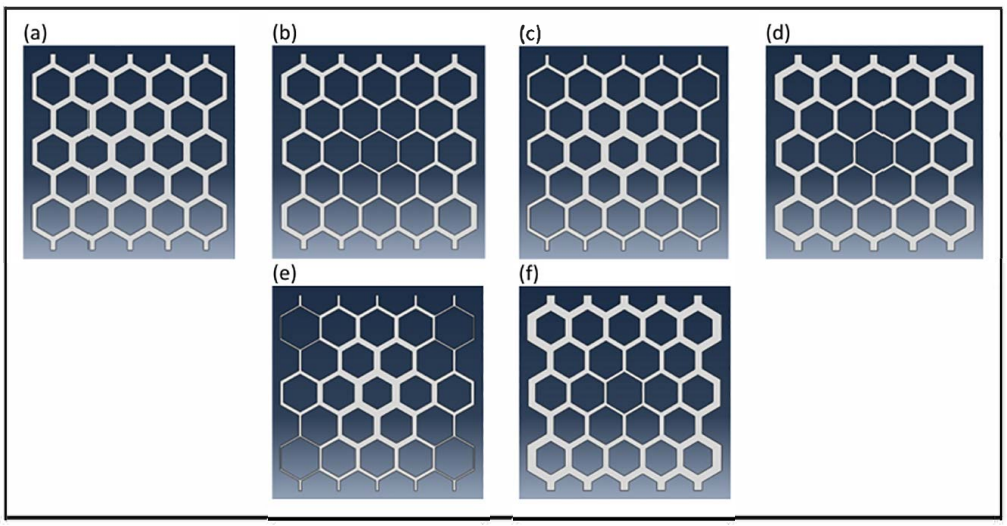

Figure 5. Graded type 3 samples with a constant height of $h = 12$ mm. The cell length varies radially among concentric layers. (a) 3A_p; (b) 3A_n; (c) 3B_p; (d) 3B_n; (e) 3C_p; (f) 3C_n.(n = negative, p = positive).

Table 4. Designation, geometrical parameters and relative density $\bar{\rho}$ for the graded type 3 structures with a constant height $h = 12$ mm.

Designation	*G parameter*	s_1 (mm)	s_2 (mm)	$\bar{\rho}$
3A_p	+0.22	89	90	0.323
3A_n	−0.22	89	90	0.240
3B_p	+0.31	89	90	0.265
3B_n	−0.31	89	90	0.298
3C_p	+0.37	89	90	0.199
3C_n	−0.37	89	90	0.335

All the regular honeycomb samples were printed, while only graded samples 2D, 3A_n and 3B_p were selected to be manufactured due to availability issues. Three samples for each arrangement were fabricated. Examples of the printed regular honeycombs specimens L6H10, L8H10 and L10H10 are shown in Figure 2(d,e,f).

Finite element modeling

The FE analysis of the compression test was conducted using the finite element analysis (FEA) software ABAQUS 2022, by Dassault Systèmes S.A. Beside the honeycomb structure, two additional cylindrical parts with a radius of 70 mm and height of 10 mm were designed, to serve as the compression plates in the simulated testing.

Two compression loading directions were evaluated meaning that the sample could be tested under in-plane conditions (Figure 6(a)) or under out-of-plane conditions (Figure 6(b)), with the cellular structure maintained between two parallel plates (Figure 6(c)) to simulate the experimental test (Figure 6(d)). The friction coefficient of the contact surfaces between the compression plates and the honeycomb structures was set as 0.2, as in previous works.[6] One plate was fixed, while the other plate was moving until a final displacement of 1.5 mm for out-of-plane testing and of 3 mm for in-plane compression, which allow capturing the final failure values. The aluminium cell-wall material was taken to be elastic-plastic. The plates were assigned as rigid with a Young's modulus ($E = 1 \times 10^{15}$ MPa), that is several orders of magnitude above the one of the aluminium alloys, to assure that no deformation occurs at the plates.

The specimens were meshed using a 10-node quadratic tetrahedral element type (C3D10). This choice comes from the fact that, in this kind of problem, quadratic elements are highly preferred as compared with linear, and also because an efficient tetrahedral mesher is embedded

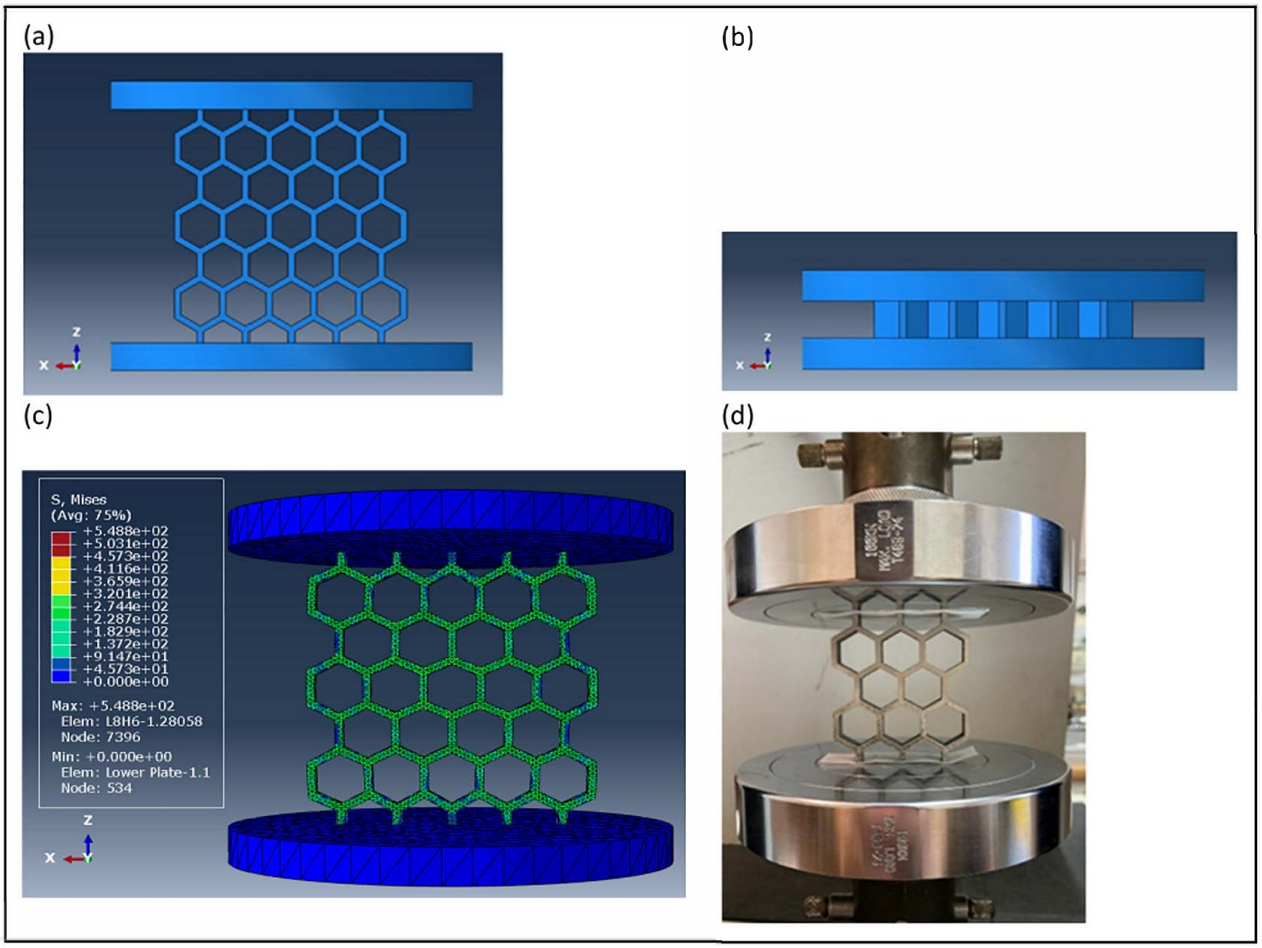

Figure 6. Cellular sample under two different compressive loading directions (a) in-plane and (b) out-of-plane; in-plane compression: (c) FEM file of sample L8H6; (d) experimental set-up of sample L10H10.

in ABAQUS. A convergence analysis was performed regarding the regular and graded honeycomb structures, ensuring the ideal number of elements while maintaining the computational process time balanced and consequently verifying the quality of the mesh. The convergence criterion was defined as less than 5% changes in the highest von Mises stress. Figure 7 shows the evolution of the maximum von Mises stress recorded in three fixed nodes over several different meshes, reaching the ideal mesh size of 1.4 mm for both regular and graded structures, corresponding to a number of elements of 34742 and 132588, respectively. The compression plates were seeded with a larger global seed size of 8 mm. Details of contact interaction properties were described in detail by B Coelho.[37]

The output variables were the displacement and reaction load, observed in the moveable compression plate, which enable the representation of the load–displacement curves. From these curves, the following parameters were calculated, namely the stiffness K, i.e. the slope of the linear initial region of the curves, the absorbed energy E_a, i.e. the area below the curves until a certain displacement (being 0.7 mm or 1.5 mm for out-of-plane and in-plane testing, respectively). Also, the maximum von Mises stress $\sigma_{\text{max von Mises}}$, and the yield stress σ_y, which

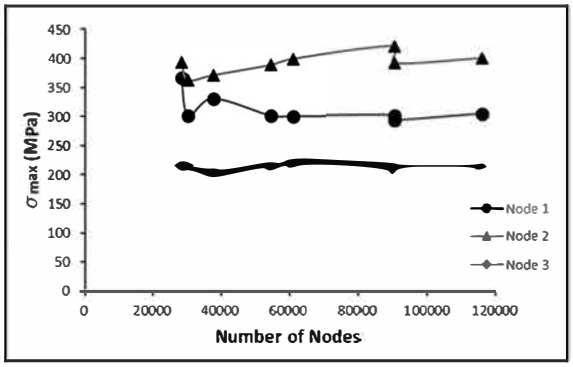

Figure 7. Convergence analysis: evolution of the von Mises stress as a function of the number of nodes for the arrangement L6H10 (in-plane) at three nodes.

corresponds to the end of the initial linear regime, were recorded. The yield stress was calculated dividing the load by the nominal area between the plate and the specimen. All the parameters were scaled with the relative density.

Experimental tests

The experimental compression tests were performed according to the standard ASTM C365-94, in an Instron

3369 universal mechanical testing machine with a load cell of 50 kN (Figure 6(b)). Three samples were used for each configuration. Both out-of-plane and in-plane tests were conducted with a cross-head speed of 0.5 mm/min. Bluehill data acquisition software was used to obtain the experimental load–displacement curves, from which the stiffness, K, and the energy, E_a, were determined. As the compression tests were conducted until failure of the samples, a failure analysis was carried out.

Results and discussion

This section starts with the presentation of results of regular honeycombs, after which results of the performance of non-regular structures are shown.

Regular structures under out-of-plane loading

Figure 8 displays the load–displacement curves obtained under compression of the regular samples when loaded along the out-of-plane direction for samples with various values of cell length l, and the cell height h. All data is numerical because there was a mismatch between numerical and experimental results. Several aspects may eventually contribute to this behaviour, such as, a large friction coefficient, the small height of the samples and their small displacement. Maybe the small height of the samples makes a more pronounced effect of the non-correction of the system compliance effects. In such cases, where the experimental displacement is measured by the cross-head displacement, due to the small deformations of the samples, the deformations in the load cell and in the overall machine set-up may induce an overestimation of the displacement. As it was not possible to apply extensometers or digital image correlation due to the small height of the samples, the authors chose to discard the experimental results for the out-of-plane loading direction, as for example, load values were more than 10 times lower in experiments than in simulations.

FE analysis as seen in Figure 8 reveals that the shape of the numerical load–displacement curves follows the same trend across all the nine arrangements, with variations in values. The results indicate that keeping the cell length constant, an increase in the sample height leads to a decrease of the applied load for the same displacement. This is in agreement with previous works.[22,40,41] In fact, Kumar et al. 2020[40] reached the conclusion that the compressive strength of cellular Ni honeycombs decreases with increasing core height, due to the mechanisms involved in the deformation. Particularly, for low core height, cell wall bending dominates, while for high core height, the deformation occurs by cell wall buckling.[40]

Table 5 shows FEA results for compression tests along the out-of-plane direction of regular structures in terms of maximum von Mises stress $\sigma_{\text{max von Mises}}$, stiffness K, absorbed energy E_a, until a displacement of 0.7 mm, and yield stress, σ_y. The yield stress is the yield load divided by the nominal cross area. However, as the number of cells on each sample is not the same, an

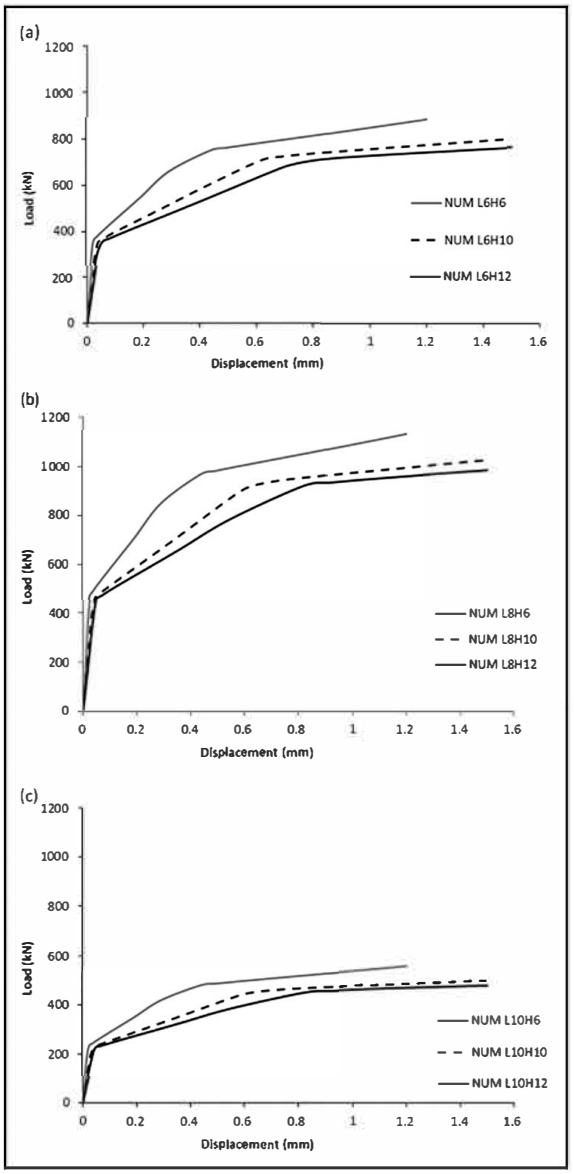

Figure 8. Numerical load-displacement curves obtained under out-of-plane loading direction for regular samples with different values of l and h.

analysis of each parameter can be biased, although the parameters were scaled with the relative density, $\bar{\rho}$. While the yield stress stands almost the same for all samples, the maximum von Mises stress tends to increase with the decrease of the relative density, not being sensitive to the variation of both l and h.

Figure 9 shows the von Mises stress distribution in a deformed sample, which reveals that some regions did not yield for this value of displacement and allows to observe the cell wall bending.

In the literature, the Young's modulus, E_3, of a regular honeycomb cellular structure, when loaded under out-of-plane conditions, is proportional to the relative density, and may be estimated by

$$E_3 = \frac{K \times h}{A} \tag{1}$$

Table 5. Fe results for compression tests out-of-plane of regular structures: maximum von Mises stress $\sigma_{max\,von\,Mises}$, stiffness K, absorbed energy E_a, until a displacement of 0.7 mm, and yield stress, σ_y (scaled with the relative density, $\bar{\rho}$). Values of E_3 calculated from equation 1.

Geometry	$\bar{\rho}$	$\sigma_{max\,von\,Mises}$ / $\bar{\rho}$ (MPa)	K / $\bar{\rho}$ (KN/mm)	E_a / $\bar{\rho}$ (J)	σ_y / $\bar{\rho}$ (MPa)	E_3 (GPa)
L6H6	0.338	1587	47368	1341	245	22.1
L6H10	0.338	1554	28679	1127	246	22.3
L6H12	0.338	1467	23468	1034	241	21.9
L8H6	0.269	2053	76164	2139	247	17.6
L8H10	0.269	2004	45641	1802	240	17.6
L8H12	0.269	2025	37841	1658	240	17.5
L10H6	0.228	2353	44853	1255	245	14.7
L10H10	0.228	2261	26799	1052	236	14.6
L10H12	0.228	2275	22247	967	236	14.6

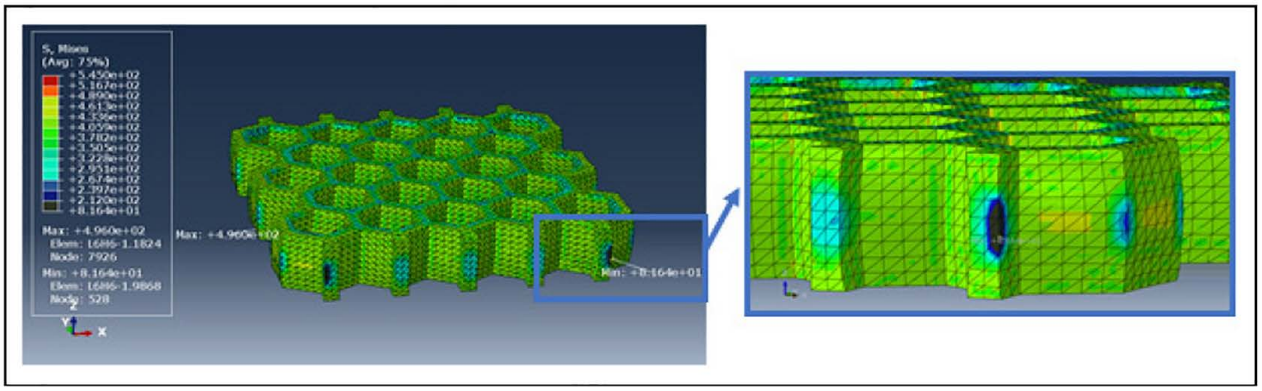

Figure 9. Illustration of the von Mises stress distribution in the deformed sample L6H6 (out-of-plane), after a displacement of 1.2 mm, showcasing a region which has not yet yielded (region in black).

where K is the stiffness, h is the core height and A is the cross-sectional or nominal area.[2,40] Indeed, the values of E_3 exhibited in Table 5 confirm that the elastic modulus increases with the relative density. Keeping the height constant and decreasing the cell length, there is an increase in the relative density and an increase in the elastic modulus E_3 (Table 5).

The core height and the cell length influence the results of regular cellular structures under out-of-plane compressive loads. An increase in core height h, leads to a decrease in both specific stiffness and specific absorbed energy, while a decrease in cell length, l, conducts to an increase of the elastic modulus.

Regular structures under in-plane loading and failure mode

Several works exit in the literature on the in-plane deformation of regular hexagonal honeycombs.[2] The results presented here are merely used for comparison purposes, namely with the ones for graded structures.

Figure 10 displays load-displacement curves obtained with regular hexagonal honeycomb samples with a fixed height of 10 mm, L6H10, L8H10 and L10H10. Both numerical and experimental results are presented in Table 6.

The mismatch between numerical and experimental results is not substantial. However, the finite element results of stiffness, absorbed energy and yield stress were found to be higher than the experimental ones. Those discrepancies may be due to non-homogeneity of the experimental specimens with defects induced by the L-PBF procedure, such as lack of fusion or key-hole cavities.[42] The porosity level, estimated by image analysis carried out on the cross section of small cubes printed at the same time as the specimens, was found to be comprised between 2.5% and 3% with the default set of parameters used. These values fall in the interval of the ones reported in the literature of 0.5 to 4%.[42] As all the pores observed had a spherical shape suggesting they were entrapped gas-type of defects, it is supposed that this relatively high porosity level could result from the presence of a small quantity of water in the powder used for the builds (number of reuse cycles < 3). Indeed, the relative humidity measured in the powder prior to its loading in the machine was comprised between 6% and 12%, even though it was left to dry overnight at 110°C beforehand. Another hypothesis could be that the entrapped gas defects are inherited from the initial powder that was obtained by nitrogen atomization. However, the porosity level of the powder was not measured.

Finally, the numerical models assume an isotropic material, which do not reflect entirely the actual properties of additively manufactured specimens as reported by other authors.[34–36] Such specimen often have an heterogeneous

Table 6. Fe results for compression tests in-plane of regular structures: maximum von Mises stress $\sigma_{max\,von\,Mises}$, stiffness K, absorbed energy E_a, until a displacement of 1.5 mm, and yield stress, σ_y (scaled with the relative density, $\bar{\rho}$).

Geometry	$\bar{\rho}$	$\sigma_{max\,von\,Mises}/\bar{\rho}$ (MPa)	$K/\bar{\rho}$ (KN/mm)		$E_a/\bar{\rho}$ (J)		$\sigma_y/\bar{\rho}$ (MPa)	
		NUM	NUM	EXP	NUM	EXP	NUM	EXP
L6H10	0.338	1504	109	49 ± 2.8	64	44 ± 1.1	59	55 ± 3.3
L8H10	0.269	1888	71	38 ± 1.4	51	36 ± 3.0	42	37 ± 2.1
L10H10	0.228	2319	40	26 ± 1.7	28	21 ± 1.8	28	23 ± 1.2

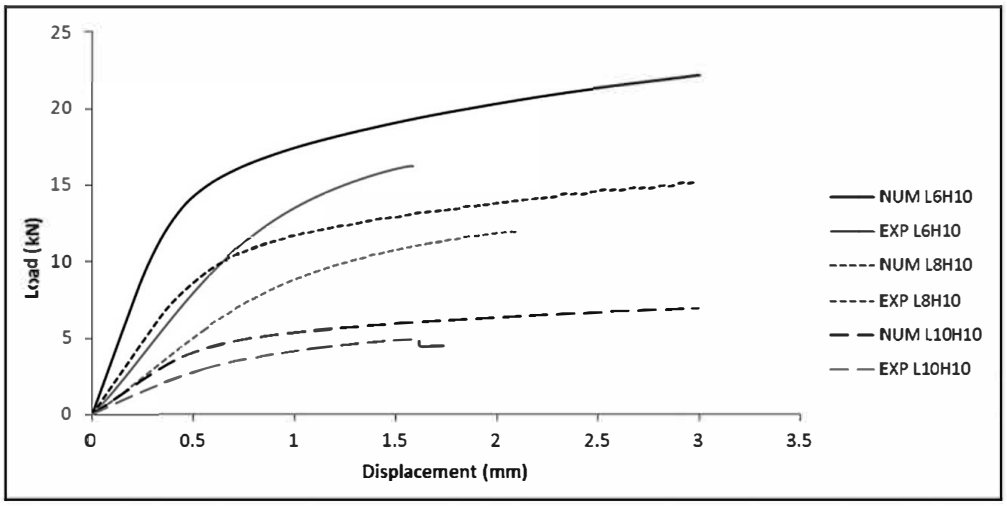

Figure 10. Load-displacement curves obtained under in-plane loading direction for regular samples with different values of l ($h = 10$ mm): numerical and experimental results for L6H10, L8H10 and L10H10.

microstructure and contains relatively high levels of residual stress that resulted from the very high thermal gradients and fast cooling speed involved in the L-PBF process. The presence of residual stress within the samples could also explain the lower mechanical performance observed in experimental tests compared to numerical simulation.[43–45]

Comparing the values obtained under out-of-plane (Table 5) with those of in-plane loading (Table 6) one can reach the conclusion that while the maximum von Mises stress remains almost the same, the scaled stiffness, absorbed energy and yield stress present much higher values in the former case, for the same relative density. This is in agreement with previous works.[46] For example, on Nomex honeycombs the yield stress may be 10 times more in the out-of-plane direction than in the in-plane loading.[46] This is a limitation of the hexagonal honeycombs that achieve high stiffness and strength under out-of-plane compression, but they show low in-plane stiffness and strength.[2] This behaviour is due to the deformation mechanisms of the cell walls that compress under out-of-plane loading and suffer bending or buckling under in-plane compression.[2]

Figure 11 presents both the simulated maximum plastic strain and the experimental failure of samples. For these aluminum samples, the collapse occurs with the fracture of the triple joints (Figure 11(g) and (h)). Failure zones present the same localization both in the experimental and in simulation data, apart from experimental sample L6H10 (Figure 11(b)), where there could be a boundary effect of the compression plate. Still, the failure of sample L6H10 also occurs at triple joints.

The failure of regular hexagonal honeycombs is strongly dependent upon the loading direction, which for the loaded conditions of Figure 11, previous research indicates that failure starts to occur at the mid-section of the sample.[2,5,46] In the current work, apart from the previously mentioned Figure 11(b), all the other samples start collapsing starts at the mid-section, as reported in the literature.

Graded structures under out-of-plane loading

The numerical load-displacement curves for all graded samples are exhibited in Figure 12, while the subsequent results are indicated in Table 7.

One may infer that the scaled stiffness and absorbed energy are clearly influenced by the cell thickness distribution, presenting smaller values of such parameters for graded 3 samples, followed by group graded 1 and finally from the set of graded 2 specimens. For the other parameters, such as the maximum von Mises stress and yield stress, there are no such clear trends. The higher values of stiffness and absorbed energy were obtained for samples graded 2A, 2B, 2C and 2D. One can notice that the relative density also increases in the group sequence of graded 3, graded 1 and graded 2.

Samples 1A, 3A_p and 3C_n have almost the same relative density, with values in the interval 0.322–0.335, but

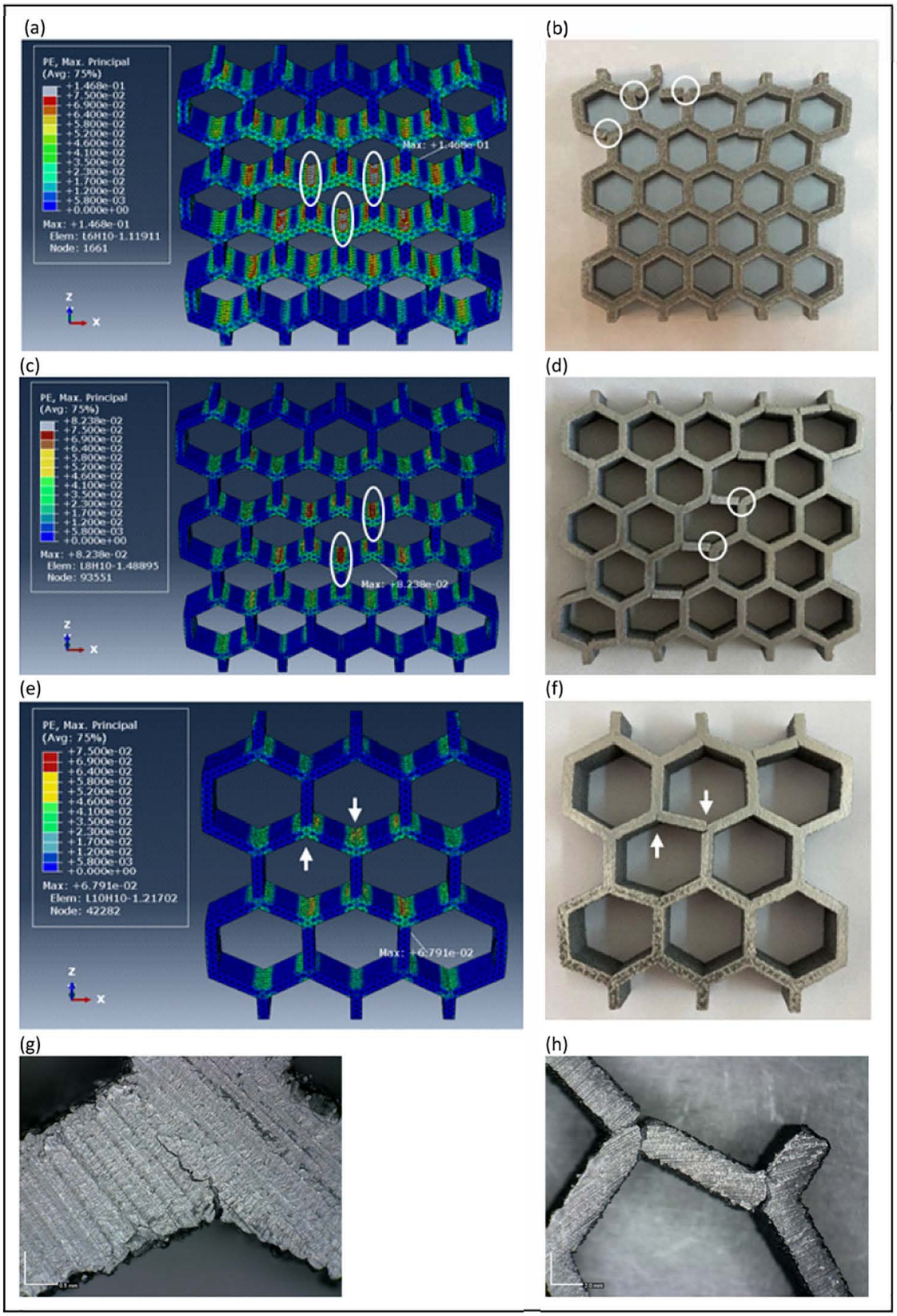

Figure 11. In-plane simulated (maximum plastic strain, PE) and experimental deformed regular samples, respectively, for: (a)(b) L6H10; (c)(d) L8H10; (e)(f) L10H10; (g) crack initiation and propagation in a triple junction (sample L10H10); (h) fracture of a collapsed cell (sample L6H10).

have different cell thickness distributions. The results from Table 7 indicate that both maximum von Mises stress $\sigma_{\text{max von Mises}}$, stiffness K, absorbed energy E_a, and yield stress, σ_y (scaled with the relative density, $\bar{\rho}$), are different among each other, for the three mentioned samples. The same behaviour is noticed for samples 1B and 2C with a

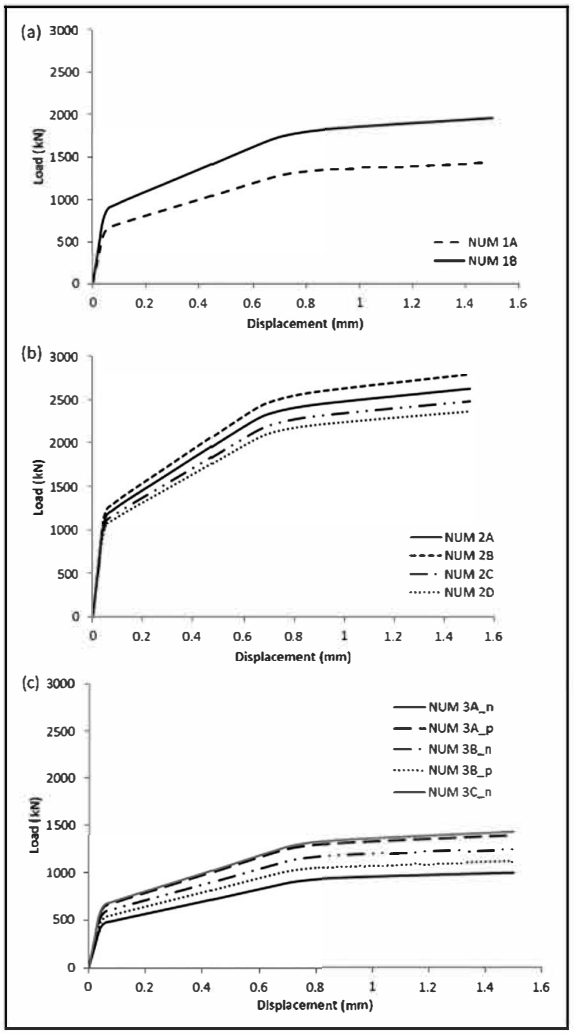

Figure 12. Numerical out-of-plane load-displacement curves for structures of different gradient type: (a) gradient 1 (b) gradient 2 (c) gradient 3.

Table 7. Fe results for compression tests out-of-plane of graded structures: maximum von Mises stress $\sigma_{max\ von\ Mises}$, stiffness K, absorbed energy E_a, until a displacement of 0.7 mm, and yield stress, σ_y (scaled with the relative density, $\bar{\rho}$). Only values from numerical simulations are presented.

Geometry	$\bar{\rho}$	$\sigma_{max\ von\ Mises}/\bar{\rho}$ (MPa)	$K/\bar{\rho}$ (KN/mm)	$E_a/\bar{\rho}$ (J)	$\sigma_y/\bar{\rho}$ (MPa)
1A	0.322	2087	45173	2019	246
1B	0.421	1233	45833	2096	250
2A	0.443	1098	57147	2680	266
2B	0.466	1055	56886	2685	259
2C	0.426	1153	56385	2619	270
2D	0.410	1233	56651	2613	269
3A_p	0.323	2271	43359	1954	180
3A_n	0.240	2365	42645	1879	340
3B_p	0.265	2364	43242	1933	346
3B_n	0.298	1792	42843	1903	220
3C_p	0.199	—	—	—	—
3C_n	0.335	1892	42960	1919	245

relative density of 0.42, meaning that the existence of a gradient influences the out-of-plane performance, even keeping the relative density constant.

The mechanical behaviour of regular hexagonal honeycombs (Table 5) may be compared with the results obtained for graded structures (Table 7), for structures that have the same relative density and the same height. For example, comparing the results of regular L6H12 with graded 3C_n, which possess $\bar{\rho} = 0.33$ and $h = 12$ mm, all the parameters are superior for the graded sample. The same happens when comparing samples regular L8H12 with graded 3B_p (with $\bar{\rho} = 0.269$ and $\bar{\rho} = 0.265$, respectively), where the graded samples show an improved compression performance. The current results show the same trend as those attained by Tao et al. 2017,[22] for a different type of gradient and dynamic compressive crushing. Those authors found that the in-plane graded honeycomb showed improved absorbed energy and crushing strength when compared to regular honeycomb, when loaded under out-of-plane conditions.[22]

Graded structures under in-plane loading and failure mode

Figure 13 displays the numerical and experimental load–displacement curves obtained under in-plane compression for specimens 2D, 3A_n and 3B_p. Experiments were performed with three samples for each case. As for the regular samples, the numerical curves were found to lie above the experimental curves, which may be explained in terms of the specificity of samples produced by L-PBF discussed in the previous section, that is, the presence of defects (spherical pores) and the heterogeneous microstructure. Also, possibly for the same reason, it can be observed some dispersion of the results between test repetitions of the same design, as the three experimental curves do not overlap. This is not uncommon for as-built specimens, which also exhibit high level of residual stresses in addition to some microstructural heterogeneity.[42–45]

Table 8 provides the FE results of maximum von Mises stress, stiffness, absorbed energy and yield stress (scaled with the relative density). Again, the numerical values are higher than the experimental ones.

On average, the lowest values of stiffness and absorbed energy were attained by samples with gradient 3, increasing progressively for specimens with gradient 1, to samples with gradient 2. The relative density also increases in the group sequence of graded 3, graded 1 and graded 2, suggesting a possible correlation of such parameters. On the maximum von Mises stress and yield stress, such tendency is not observed. The highest values of $K/\bar{\rho}$ and $E_a/\bar{\rho}$ were achieved by graded samples 2A, 2B, 2C and 2D.

Analysing the numerical results for samples 1A, 3A_p and 3C_n, which have almost the same relative density, one may infer that the scaled stiffness is not much

different, but the maximum von Mises stress, and absorbed energy present very distinct values. Also, samples 1B and 2C which have almost the same relative density, exhibit dissimilar results. Again, the effect of the cell thickness distribution can be seen.

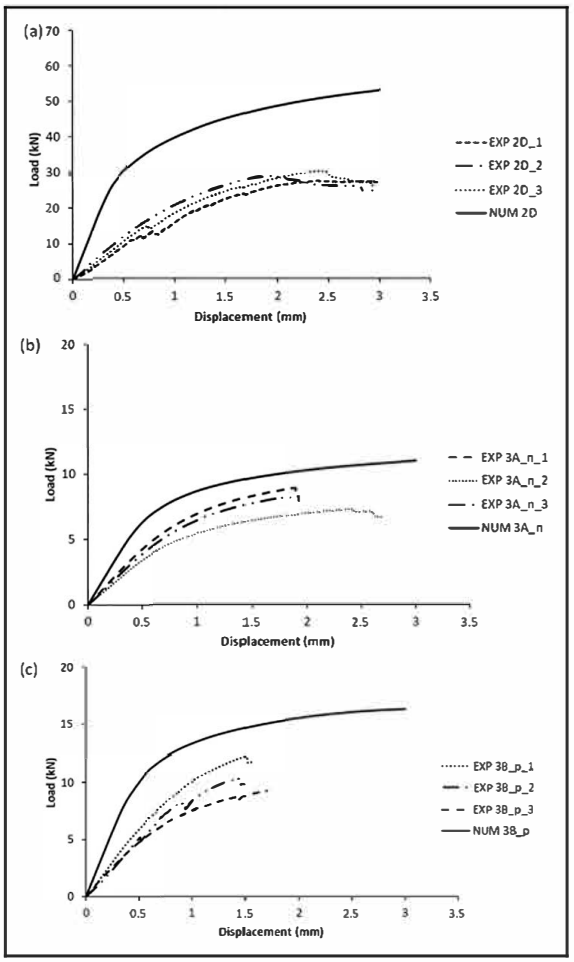

Figure 13. In-plane numerical and experimental load displacement curves for graded structures: (a) 2D; (b) 3A_n; (c) 3B_p.

The comparison of the results obtained for graded samples under out-of-plane loading (Table 7) with the in-plane loading (Table 8), reveals that the stiffness, absorbed energy and yield stress present much lower values when the compression is performed under in-plane solicitations. The maximum von Mises stress does not seem to be affected by in- or out-of-plane loading conditions.

A comparison of the results for regular and graded samples may be exemplified with samples regular L8H10 and graded 3B_p, which possess almost the same relative density, for which the values of $K/\bar{\rho}$ and $E_a/\bar{\rho}$ tend to be larger for the graded. Another example is given by comparing the regular L6H10 and graded 3A_p samples, with an increase of 34% in absorbed energy, while simultaneously presenting an inferior value for relative density The tendency that graded samples show higher values of absorbed energy in comparison with regular uniform structures was reported by other authors, although for a different type of gradient.[28]

The failure mode of graded structures strongly depends on the cell thickness distribution. Choy et al. 2017[28] report, for another type of gradient, that the collapse of structure started from least dense layer to the denser layers. This is also what happened as shown in Figure 14, which reveals that the strain distribution is not uniform along the cellular structure with highly deformed cells that corresponds to the lower thickness cells. It means that collapse by failure starts to occur at cells with smaller thickness. Simulation results are consistent with experimental observations, with failure zones occurring at the same localization both in the experimental and in simulation data. Under in-plane compression, structures with gradient present a deformation mechanism that depends on the designed cell thickness distribution.

Table 8. Results for in-plane compression tests of graded structures: maximum von Mises stress $\sigma_{max\,von\,Mises}$, stiffness K, absorbed energy E_a, until a displacement of 1.5 mm, and yield stress, σ_y (scaled with the relative density, $\bar{\rho}$). Both numerical and experimental values are presented. Experimental results are an average of three tests.

Geometry	$\bar{\rho}$	$\sigma_{max\,von\,Mises}/\bar{\rho}$ (MPa)	$K/\bar{\rho}$ (KN/mm)		$E_a/\bar{\rho}$ (J)		$\sigma_y/\bar{\rho}$ (MPa)	
		NUM	NUM	EXP	NUM	EXP	NUM	EXP
1A	0.322	2432	91	—	63	—	—	—
1B	0.421	1429	167	—	101	—	—	—
2A	0.443	1081	195	—	114	—	—	—
2B	0.466	1063	214	—	121	—	—	—
2C	0.426	1151	195	—	124	—	—	—
2D	0.410	1180	179	55 ± 3.0	116	51 ± 3.6	65	33 ± 1.9
3A_p	0.323	1528	91	—	86	—	—	—
3A_n	0.240	2394	57	34 ± 2.3	42	30 ± 2.1	28	21 ± 1.2
3B_p	0.265	2194	86	43 ± 2.2	59	37 ± 2.9	38	30 ± 2.1
3B_n	0.298	2046	82	—	56	—	—	—
3C_p	0.199	2392	49	—	34	—	—	—
3C_n	0.335	1904	100	—	65	—	—	—

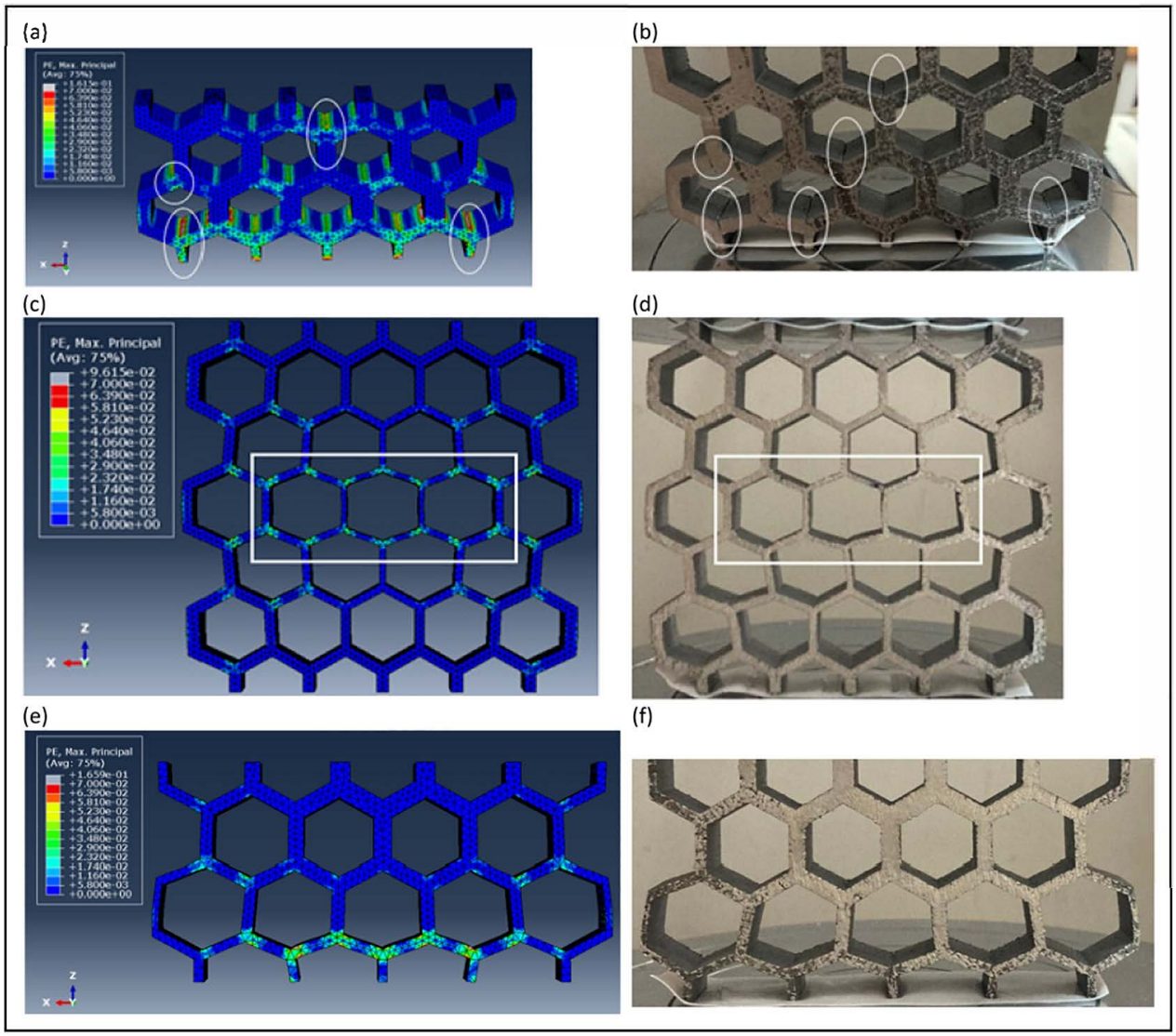

Figure 14. In-plane simulations (maximum principal plastic strain, PE) and experimental deformation of graded samples: (a) (b) sample 2D; (c) (d) sample 3A_n; (e)(f) sample 3B_p.

Conclusions

Recently, intensive research has been carried out to improve the out-of-plane and the in-plane performance of honeycombs, focusing on the control of material distribution, by varying cell sizes or cell wall thickness.

In the present work, novel in-plane radial graded hexagonal structures were designed in a pursuit of increasing both the out-of-plane and the in-plane performance of honeycombs. The compressive behaviour of the regular and graded structures was investigated using numerical simulation and experimental tests, performed with aluminium samples produced by L-PBF.

Results allow to confirm that the compressive properties of regular honeycombs loaded under out-of-plane direction were influenced by the core height and cell length, which is an in-plane characteristic. The study also confirmed that the stiffness, absorbed energy and strength are much higher for the out-of-plane loading in comparison with the in-plane loading, for regular honeycombs with the same relative density.

Graded samples that possess different cellular thickness distribution, but have the same relative density, exhibit different values of stiffness, absorbed energy and strength, under out-of-plane loading. This means that the cell thickness arrangement on the in-plane, influences the out-of-plane results. Also, the data achieved by out-of-plane loadings shows that graded structures exhibit higher mechanical performance when compared with regular honeycombs. Graded arrangements have lower mechanical properties when loaded in the in-plane direction than in the out-of-plane direction.

The in-plane loading of graded samples leads to higher values of the mechanical properties in comparison with regular honeycombs. The failure mode is different for regular and graded specimens. Regular arrangements start to fail at the mid-section, while graded samples start to collapse at the lowest thickness cell walls, whose location varies from one gradient to another. Also, the existence of graded structures enables to tailor the spots for a specific localization of deformation.

This research allows concluding that a particular gradient profile of cell wall thickness can be explored to obtain stiffness, absorbed energy and failure modes specific to requested applications, typically higher than such for their regular hexagonal counterparts.

Acknowledgements

This work was supported by FCT, through IDMEC, under LAETA, Project UIDB/50022/2020 with DOI: 10.54499/UIDB/50022/2020. A. M. Deus was partially supported by CeFEMA Project No. UIDB/04540/2020. Both projects are sponsored by FCT, the Portuguese Agency for Science and Technology.

Declaration of conflicting interests

The authors declared no potential conflicts of interest with respect to the research, authorship and/or publication of this article.

Funding

The authors disclosed receipt of the following financial support for the research, authorship and/or publication of this article: This work was supported by the Fundação para a Ciência e a Tecnologia (grant numbers CeFEMA Project No. UIDB/04540/2020, IDMEC, LAETA, Project UIDB/50022/2020).

ORCID iD

Augusto Moita Deus https://orcid.org/0000-0002-0451-6245
Maria Fatima Vaz https://orcid.org/0000-0003-1629-523X

References

1. Bitzer T. *Honeycomb technology: material design, manufacturing applications and testing*. New York: Springer, 1997.
2. Gibson LJ and Ashby MF. *Cellular solids: structure and properties*. 2nd ed. Cambridge: Cambridge University Press, 1997.
3. Xu S, Beynon JH, Ruan D, et al. Experimental study of the out-of-plane dynamic compression of hexagonal honeycombs. *Compos Struct* 2012; 94: 2326–2336.
4. Araújo H, Leite M, Ribeiro AR, et al. The effect of geometry on the flexural properties of cellular core structures. *Proc Inst Mech Eng Part L J Mater Des Appl* 2019; 233: 338–347.
5. Araújo H, Leite M, Ribeiro A, et al. Investigating the contribution of geometry on the failure of cellular core structures obtained by additive manufacturing. *Frat ed Integrità Strutt* 2019; 13: 478–486.
6. Miranda A, Leite M, Reis L, et al. Evaluation of the influence of design in the mechanical properties of honeycomb cores used in composite panels. *Proc Inst Mech Eng Part L J Mater Des Appl* 2021; 235: 1325–1340.
7. Zhang J, Wang Z and Zhao L. Dynamic response of functionally graded cellular materials based on the Voronoi model. *Compos Part B Eng* 2016; 85: 176–187.
8. Habib FN, Iovenitti P, Masood SH, et al. In-plane energy absorption evaluation of 3D printed polymeric honeycombs. *Virtual Phys Prototyp* 2017; 12: 117–131.
9. Yang X, Ma J, Shi Y, et al. Crashworthiness investigation of the bio-inspired bi-directionally corrugated core sandwich panel under quasi-static crushing load. *Mater Des* 2017; 135: 275–290.
10. Townsend S, Adams R, Robinson M, et al. 3D printed origami honeycombs with tailored out-of-plane energy absorption behavior. *Mater Des* 2020; 195: 108930.
11. Zhang Z, Zhang Q, Zhang D, et al. Enhanced mechanical performance of brazed sandwich panels with high density square honeycomb-corrugation hybrid cores. *Thin-Walled Struct* 2020; 151: 106757.
12. Geramizadeh H, Dariushi S and Salami SJ. Numerical and experimental investigation for enhancing the energy absorption capacity of the novel three-dimensional printed sandwich structures. *Proc Inst Mech Eng Part L J Mater Des Appl* 2021; 235: 1622–1634.
13. Oliveira A, et al. Evaluation of cellular structures with triply periodic minimal surfaces fabricated by additive manufacturing. *Eng Manuf Lett* 2022; 1: 28–33.
14. Benedetti M, du Plessis A, Ritchie RO, et al. Architected cellular materials: a review on their mechanical properties towards fatigue-tolerant design and fabrication. *Mater Sci Eng R: Reports* 2021; 144: 100606.
15. Monteiro J, et al. Evaluation of the effect of core lattice topology on the properties of sandwich panels produced by additive manufacturing. *Proc Inst Mech Eng Part L J Mater Des Appl* 2021; 235: 1312–1324.
16. Al-Ketan O, Soliman A, AlQubaisi AM, et al. Nature-inspired lightweight cellular co-continuous composites with architected periodic gyroidal structures. *Adv Eng Mater* 2018; 20: 1700549.
17. Ullah I, Brandt M and Feih S. Failure and energy absorption characteristics of advanced 3D truss core structures. *Mater Des* 2016; 92: 937–948.
18. Zama C, Chinga-Carrasco G and Echtermeyer AT. Bending properties and numerical modelling of cellular panels manufactured from wood fibre/PLA biocomposite by 3D printing. *Compos Part A Appl Sci Manuf* 2023; 165: 107368.
19. Yazdani Sarvestani H, Akbarzadeh AH, Mirbolghasemi A, et al. 3D printed meta-sandwich structures: failure mechanism, energy absorption and multi-hit capability. *Mater Des* 2018; 160: 179–193.
20. Park K-M, Min K-S and Roh Y-S. Design optimization of lattice structures under compression: study of unit cell types and cell arrangements. *Materials (Basel)* 2021; 15: 97.
21. Garrido Silva B, et al. Functionally graded cellular cores of sandwich panels fabricated by additive manufacturing. *Proc Inst Mech Eng Part L J Mater Des Appl* 2022; 236: 1814–1828.
22. Tao Y, Duan S, Wen W, et al. Enhanced out-of-plane crushing strength and energy absorption of in-plane graded honeycombs. *Compos Part B Eng* 2017; 118: 33–40.
23. Shen CJ, Lu G and Yu TX. Dynamic behavior of graded honeycombs – a finite element study. *Compos Struct* 2013; 98: 282–293.
24. Wang X, Zheng Z and Yu J. Crashworthiness design of density-graded cellular metals. *Theor Appl Mech Lett* 2013; 3: 031001.
25. Zhang Y, Lu M, Wang CH, et al. Out-of-plane crashworthiness of bio-inspired self-similar regular hierarchical honeycombs. *Compos Struct* 2016; 144: 1–13.
26. Limmahakhun S, Oloyede A, Sitthiseripratip K, et al. Stiffness and strength tailoring of cobalt chromium graded cellular structures for stress-shielding reduction. *Mater Des* 2017; 114: 633–641.

27. Zhang S, Li C, Hou W, et al. Longitudinal compression behavior of functionally graded Ti-6Al-4V meshes. *J Mater Sci Technol* 2016; 32: 1098–1104.
28. Choy SY, Sun C-N, Leong KF, et al. Compressive properties of functionally graded lattice structures manufactured by selective laser melting. *Mater Des* 2017; 131: 112–120.
29. Bates SRG, Farrow IR and Trask RS. Compressive behaviour of 3D printed thermoplastic polyurethane honeycombs with graded densities. *Mater Des* 2019; 162: 130–142.
30. Liu H, Zhang ET and Ng BF. In-plane dynamic crushing of a novel honeycomb with functionally graded fractal self-similarity. *Compos Struct* 2021; 270: 114106.
31. Frazier WE. Metal additive manufacturing: a review. *J Mater Eng Perform* 2014; 23: 1917–1928.
32. Wei K, et al. Mechanical analysis and modeling of metallic lattice sandwich additively fabricated by selective laser melting. *Thin-Walled Struct* 2020; 146: 106189.
33. Stocchi A, Colabella L, Cisilino A, et al. Manufacturing and testing of a sandwich panel honeycomb core reinforced with natural-fiber fabrics. *Mater Des* 2014; 55: 394–403.
34. Croccolo D, De Agostinis M and Olmi G. Experimental characterization and analytical modelling of the mechanical behaviour of fused deposition processed parts made of ABS-M30. *Comput Mater Sci* 2013; 79: 506–518.
35. Leite M, Varanda A, Ribeiro AR, et al. Mechanical properties and water absorption of surface modified ABS 3D printed by fused deposition modelling. *Rapid Prototyp J* 2018; 24: 195–203.
36. Rybachuk M, Alice Mauger C, Fiedler T, et al. Anisotropic mechanical properties of fused deposition modeled parts fabricated by using acrylonitrile butadiene styrene polymer. *J Polym Eng* 2017; 37: 699–706.
37. Bernardo Capelo Coelho. Modeling and Characterization of Honeycomb Structures with Density Gradient Produced by Additive Manufacturing Technologies. Instituto Superior Técnico, Universidade de Lisboa; 2022.
38. SLM Solutions. Al-Alloy AlSi7Mg0,6 Material Data Sheet; 2023.
39. SLM. [Online]. Available: https://www.slm-solutions.com/company/about-us. [Accessed: 15-Mar-2024].
40. Kumar SS, Rao MS, Balasundar I, et al. Compressive behaviour of a nickel superalloy Superni 263 honeycomb sandwich panel. *J Sandw Struct Mater* 2020; 22: 1426–1449.
41. Zhang J and Ashby MF. The out-of-plane properties of honeycombs. *Int J Mech Sci* 1992; 34: 475–489.
42. de Terris T, et al. Optimization and comparison of porosity rate measurement methods of selective laser melted metallic parts. *Addit Manuf* 2019; 28: 802–813.
43. Chen C, Chang S, Zhu J, et al. Residual stress of typical parts in laser powder bed fusion. *J Manuf Process* 2020; 59: 621–628.
44. Chen Z, et al. Ductility enhancement of additively manufactured CoCrMo alloy via residual stress tailored high stacking fault probability. *Scr Mater* 2023; 235: 115626.
45. Levkulich NC, Semiatin SL, Gockel JE, et al. The effect of process parameters on residual stress evolution and distortion in the laser powder bed fusion of Ti-6Al-4V. *Addit Manuf* 2019; 28: 475–484.
46. Xie S, Feng Z, Zhou H, et al. In-plane and out-of-plane compressive mechanical properties of Nomex honeycombs and their prediction. *J Braz Soc Mech Sci Eng* 2020; 42: 460.